

Review

Machine Learning Techniques for Gully Erosion Susceptibility Mapping: A Review

Hamid Mohebzadeh ¹, Asim Biswas ², Ramesh Rudra ¹ and Prasad Daggupati ^{1,*}¹ School of Engineering, University of Guelph, Guelph, ON N1G2W1, Canada² School of Environmental Sciences, University of Guelph, Guelph, ON N1G2W1, Canada

* Correspondence: pdaggupa@uoguelph.ca

Abstract: Gully erosion susceptibility mapping (GESM) through predicting the spatial distribution of areas prone to gully erosion is required to plan gully erosion control strategies relevant to soil conservation. Recently, machine learning (ML) models have received increasing attention for GESM due to their vast capabilities. In this context, this paper sought to review the modeling procedure of GESM using ML models, including the required datasets and model development and validation. The results showed that elevation, slope, plan curvature, rainfall and land use/cover were the most important factors for GESM. It is also concluded that although ML models predict the locations of zones prone to gully erosion reasonably well, performance ranking of such methods is difficult because they yield different results based on the quality of the training dataset, the structure of the models, and the performance indicators. Among the ML techniques, random forest (RF) and support vector machine (SVM) are the most widely used models for GESM, which show promising results. Overall, to improve the prediction performance of ML models, the use of data-mining techniques to improve the quality of the dataset and of an ensemble estimation approach is recommended. Furthermore, evaluation of ML models for the prediction of other types of gully erosion, such as rill-interill and ephemeral gully should be the subject of more studies in the future. The employment of a combination of topographic indices and ML models is recommended for the accurate extraction of gully trajectories that are the main input of some process-based models.

Keywords: gully erosion susceptibility mapping (GESM); machine learning; support vector machine; random forest



Citation: Mohebzadeh, H.; Biswas, A.; Rudra, R.; Daggupati, P. Machine Learning Techniques for Gully Erosion Susceptibility Mapping: A Review. *Geosciences* **2022**, *12*, 429. <https://doi.org/10.3390/geosciences12120429>

Academic Editors: Ingrid Luffman and Jesus Martinez-Frias

Received: 17 October 2022

Accepted: 17 November 2022

Published: 22 November 2022

Publisher's Note: MDPI stays neutral with regard to jurisdictional claims in published maps and institutional affiliations.



Copyright: © 2022 by the authors. Licensee MDPI, Basel, Switzerland. This article is an open access article distributed under the terms and conditions of the Creative Commons Attribution (CC BY) license (<https://creativecommons.org/licenses/by/4.0/>).

1. Introduction

Gully erosion is one of the most important forms of erosion that causes land degradation problems by reducing the quality and quantity of arable soil in both developed and developing countries [1,2]. Gullies are categorized into two types, namely, “permanent” and “ephemeral” gullies [3]. Permanent gullies are commonly described as erosion channels with a depth of 0.5 to 30 m or a cross-sectional area larger than 0.09 m² [4,5] that cannot be obliterated by conventional tillage due to their large size [6,7]. By contrast, ephemeral gullies are small channels that are formed due to the results of natural and concentrated flow which can be removed by normal tillage [3]. Generally, the negative effects of gullies can be aggravated by rapid changes in soil characteristics resulting from land use change and agricultural pressure through expansion of farming activities and intensive grazing [1,8–11].

There is unanimity in the literature that the prediction of gully erosion trajectories (trajectory is defined as the exact location and path of the gully) and the estimation of soil loss from gullies would provide planners with important information for implementing erosion control strategies in agricultural watersheds [12–15]. Different studies have demonstrated that the initiation and development of gullies are mostly controlled by precipitation, topographic features, soil condition and land use/land management practices [16–19].

Hence, various process-based models (e.g., chemicals, runoff and erosion from agricultural management systems (CREAMS) [20], the ephemeral gully erosion model (EGEM) [21], groundwater loading effects of agricultural management systems (GLEAMS) [22,23], the revised ephemeral gully erosion model (REGEM) [24], the water erosion prediction project (WEPP) [25], and annualized agricultural non-point source (AnnAGNPS) [26]) have been developed to use these factors to quantify soil loss from gully erosion. However, measurements of the input factors, which are the basic requirements of the process-based models are not generally available on a larger scale. For example, the CREAMS model needs the original length of the gully to compute the amount of sedimentation [20], which limits its application for large scale areas where the measured lengths of gullies are not available.

Topographic indices (e.g., slope-area (SA) [27], the compound topographic index (CTI) [28] and the topographic wetness index (TWI) [29]) have been developed to predict gully trajectories that can be used as the input to process-based models for the estimation of soil loss due to gully erosion. Topographic indices predict gully trajectories based on the assumption that gully formation can be related to the combined effects of the main topographic characteristics [30]. Although topographic indices show promising potential for the identification of the exact location of gullies, they only consider topographic factors and do not account for rainfall characteristics, land use or soil properties which is a major limitation that leads to simplistic representations of gully formation [31–33].

Recent studies indicate that remote sensing can supply good data for analyzing and predicting gully trajectories [34–39]. Remote sensing not only provides the input data (e.g., digital elevation models (DEMs)) for topographic index models [16,40,41] and process-based models [42], but can also be used individually for the detection of gully trajectories by visual interpretation. Gully trajectories can be detected by manual digitization or interpretation of gullies from aerial photos or satellite images. For example, Wang, et al. [43] used multi-source remote sensing data to map the spatial distribution of gully trajectories at different spatial scales (Pleiades 1A, 0.7 m; unmanned aerial vehicle (UAV), 0.042 m). To identify gully trajectories, they used visual interpretation and field verification; the results obtained showed that the sub-meter images were a good source of data for the identification of various gully types, and that using satellite and UAV data simultaneously provided satisfactory gully erosion assessment at multiple spatial scales. In another study, Zhang, et al. [44] applied visual interpretation of topographical maps using Landsat enhanced thematic mapper plus (ETM+) images and SPOT-5 satellite images to map gully trajectories in the Kebai region, China. The results obtained showed that gullies had the greatest density in hilly and tableland regions and the lowest density in flatlands.

Although UAV data provide satisfactory results for detailed gully trajectory mapping at the site scale, due to limitations, such as vulnerability to weather conditions and overall budget problems, they are not suitable for large scales. On the other hand, as reported by Skyland [45], the use of remote-sensing information from a particular satellite is growing dramatically by several terabytes per day and global gathered observation data may exceed one exabyte [46]. Therefore, due to the high volume of remote-sensing data, analyzing and visually interpreting the information provided by remote-sensing imagery is beyond human abilities to process and is also costly and labor-intensive [47–49]. Therefore, advanced techniques are required that can adapt to the challenges associated with analyzing remote-sensing data.

Many studies have demonstrated the ability of machine learning (ML) algorithms to discover the rules and patterns in large datasets [50]. Hence, over the past few years, an increasing number of ML applications have been developed in geology [51,52], forestry [53–55], hydrology [56–58], agriculture [59–61], and other domains, such as soil-erosion studies [62–64].

Many technical papers are available that use ML techniques for identifying areas prone to gully erosion via gully erosion susceptibility mapping (GESM). Susceptibility is defined as the potential of a specific landscape to be influenced by a particular erosion process or a group of erosion processes [65]. To use ML algorithms efficiently in the field of GESM, four main questions must be answered: (1) What are the main steps for

developing an accurate ML model for GESM? (2) What are the best predictor variables for GESM? (3) What spatial resolution of data can be used to produce accurate detection of gullies? (4) What is the best ML model to be used for GESM? However, among the different technical papers in the field of GESM, no study provides explicit answers to these questions because related studies test the ML models over different regions with different environmental conditions and the results of one study cannot be directly used in another study. Therefore, the main objective of the current paper is to present a thorough review of the literature on ML models and approaches currently used for GESM, especially those producing susceptibility maps of permanent gullies, to facilitate user selection among ML models, predictor variables and their spatial resolution and model development for effective GESM. The paper is organized as follows: Section 2 presents a brief discussion of some basic concepts applicable to widely used ML techniques. Section 3 describes and discusses the common ML methodologies used in GESM studies. Section 4 is dedicated to comparative performance analysis of various ML models applied to GESM. Section 5 presents the conclusion and recommendations. Table 1 provides a list of the abbreviations used in the paper.

Table 1. Summary table of the abbreviations used (in alphabetical order) in the current paper.

Abbreviation	Definition	Abbreviation	Definition
ADTree	Alternating Decision Tree	GLEAMS	Groundwater Loading Effects of Agricultural Management Systems
ALOS	Advanced Land Observing Satellite	GPS	Global Positioning System
ANN	Artificial Neural Network	GWR	Geographically Weighted Regression
AnnAGNPS	Annualized Agricultural Non-Point Source	LMT	Logistic Model Tree
ASTER	Advanced Spaceborne Thermal Emission and Reflection Radiometer	MAE	Mean Absolute Error
AUC	Area Under the ROC Curve	ML	Machine Learning
AW3D30	World 3D-30 m	MLFF-ANN	Multi-Layer Feed-Forward ANN
BP	Back Propagation	MLP	Multilayer Perceptron Neural Network
BRT	Boosted Regression Tree	NBTree	Naïve Bayes Tree
CART	Classification And Regression Trees	NPV	Negative Predictive Value
CCE	Calcium Carbonate Equivalent	OOB	Out-Of-Bag
CDT-ADTree	Credal Decision Tree-Alternative Decision Tree	PPV	Positive Predictive Value
CDT-BA	Credal Decision Tree-Bagging	RBF	Radial Basis Function
CDT-DA	Credal Decision Tree-Dagging	REGEM	Revised Ephemeral Gully Erosion Model
CDT-RF	Credal Decision Tree Rotation Forest	RF	Random Forest
Cforest	Conditional Inference Forests	RMSE	Root Mean Square Error
CF	Certainty Factor	ROC	Receiver Operating Characteristic
CREAMS	Chemicals, Runoff, and Erosion from Agricultural Management Systems	SA	Slope-Area
CTI	Compound Topographic Index	SLFF-ANN	Single-Layer Feed-Forward ANN
DEMs	Digital Elevation Models	SOC	Soil Organic Carbon
DLNN	Deep Learning Neural Network	SRTM	Shuttle Radar Topography Mission
DS-BL	DS-Binary Logistic	SVM	Support Vector Machine
DS-BLW	DS-Binary Logitraw	TN	True Negative
DS-RL	DS-Reg Linear	TN	Tree Net
DS-RLG	DS-Reg Logistic	TOL	Tolerance
EGEM	Ephemeral Gully Erosion Model	TP	True Positive
ETM+	Landsat Enhanced Thematic Mapper Plus	TPI	Topographic Position Index
FN	False Negative	TSS	True Skill Statistic
FP	False Positive	TWI	Topographic Wetness Index
GEFs	Geo-Environmental Factors	UAV	Unmanned Aerial Vehicle
GEIM	Gully Erosion Inventory Map	VIF	Variance Inflation Factor
GESM	Gully Erosion Susceptibility Mapping	WEPP	Water Erosion Prediction Project
GESMs	Gully Erosion Susceptibility Maps	XGBoost	Extreme Gradient Boosting

2. Machine Learning Techniques Used in GESM

ML is a branch of computer science that is used for data analysis. It is also classified as an artificial intelligence method since it enables computers to learn from experiences in a similar way to humans or animals. In other words, ML techniques use computational methods to capture the relationship between predictors and targets without using a predefined equation as a model [66]. This capability of ML models makes them flexible techniques for solving non-linear problems with a large number of datasets from multiple sources [49]. Typically, ML problems are categorized into two main classes: (i) supervised and (ii) unsupervised learning. In supervised learning, the model is trained on known inputs and the corresponding outputs to establish a rule which is used for the prediction of future outputs [67]. In unsupervised learning, input data is processed to discover hidden patterns or intrinsic structures in input data. Figure 1 shows the classification of the ML techniques and the most commonly used models related to each category.

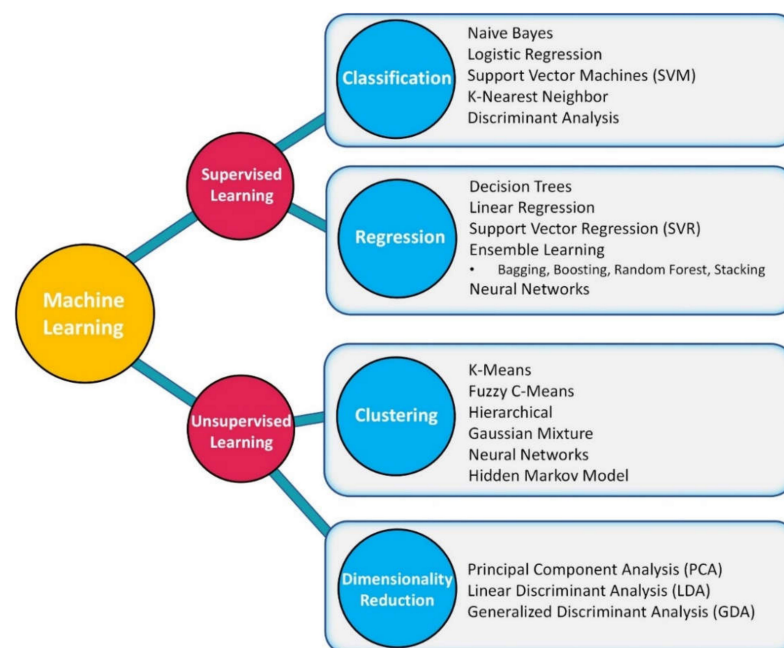


Figure 1. Classification of ML techniques.

Generally, the main objective of ML models is to map a set of “explanatory” or “predictor” variables $x = \{x_1, \dots, x_n\}$ to an “output” or “predictand” variable y using a set of “training” samples $\{y_i, x_i\}_i^N$ to obtain an approximate $f(x)$ that minimizes the error between y and $\hat{y} = f(x)$ [66]. Different error functions are used to compute the error between y and $\hat{y} = f(x)$, but the most used functions are squared-error $(y-\hat{y})^2$ for regression and negative binomial log-likelihood for classification. There are various ML techniques in the literature that are used in the field of classification and regression or both; however, only the classification types which are applied for gully erosion identification are explained in the current review.

2.1. Random Forest

Random forest (RF), developed by [68], is a rapid learning algorithm that is used for regression and classification problems. In RF, various trees are produced by the algorithm and combined to form a forest. This procedure is based on the assumption that various prediction models could produce more accurate results than one model [69]. To increase the performance accuracy of the model, a classification and regression trees (CART) technique is used to define each tree based on a bootstrapped sample of the dataset [70]. The CART technique repeats k times to define the trees using a random subgroup of the variables chosen at each node [71]. A majority vote is applied to all the trees to compute the

final results of the model [69,72]. The main interesting features of RF are that it (i) is a robust algorithm that avoids overfitting, (ii) shows low bias and low variance because of computation of the average over a large number of trees, (iii) provides strong estimation of errors using out-of-bag (OOB) data, and (iv) offers higher estimation performance [73,74].

2.2. Support Vector Machine

Support vector machine (SVM) is a control learning method proposed by Cortes and Vapnik [75]. SVM is a powerful method due to its capability for working with non-linear data and minimizes complexity [76]. SVM applies statistical learning theory and uses a mathematical process to obtain an optimal hyperplane that creates the maximum margin between two classes to separate them [77,78]. The following optimization problem is solved to find the optimal hyperplane:

$$\begin{aligned} & \text{Min} \sum_{i=1}^n \alpha_i - \frac{1}{2} \sum_{i=1}^n \sum_{j=1}^n \alpha_i \alpha_j y_i y_j (x_i x_j) \\ & \text{Subject to} \sum_{i=1}^n \alpha_i y_i = 0 \text{ and } 0 \leq \alpha_i \leq C \end{aligned} \tag{1}$$

where α_i are the Lagrange multipliers and C denotes the penalty factor. Typically, when dealing with non-linear data, SVM uses techniques called kernel functions. Kernel functions can transfer data from a lower-dimensional space to a higher-dimensional space [79,80]. Although various kernel functions have been proposed, based on the literature, four kernel types, including the radial basis function (RBF), and linear, polynomial, and sigmoid functions, are the most used functions [81,82].

2.3. Alternating Decision Tree

The alternating decision tree (ADTree) is a model which incorporates the decision tree with boosting algorithm [83]. Some studies have demonstrated that the ADTree model produces better accuracy than the standard model trees in classification problems [84]. Generally, in ADTree, two types of nodes, including a splitter node and a prediction node, are used instead of each decision node. The splitter node defines the data based on the selected attribute values, while the prediction node includes the real-valued number, which is used for prediction [83,85]. At each boosting iteration, two sets, including a set of preconditions (P_t) and a set of base rules (R_t), are maintained by the algorithm. The base rules that generate preconditions can be any real numbers, including a prediction c_1 , a base condition c_2 , and two real numbers, a and b .

The first rule R_1 is set to have a true precondition and condition; the first prediction value can be defined as:

$$a = \frac{1}{2} \ln \frac{W_+(True)}{W_-(True)} \tag{2}$$

Then c_1 and c_2 are selected by minimizing $Z_t(c_1, c_2)$:

$$Z_t(c_1, c_2) = 2 \left(\sqrt{W_+(c_1 \wedge c_2) W_-(c_1 \wedge c_2)} + \sqrt{W_+(c_1 \wedge \neg c_2) W_-(c_1 \wedge \neg c_2)} \right) + W(-c_2) \tag{3}$$

The prediction is a when $c_1 \wedge c_2$ or b when $c_1 \wedge \neg c_2$. The values of a and b are computed with the following formula:

$$a = \frac{1}{2} \ln \frac{W_+(c_1 \wedge c_2)}{W_-(c_1 \wedge c_2)}, b = \frac{1}{2} \ln \frac{W_+(c_1 \wedge \neg c_2)}{W_-(c_1 \wedge \neg c_2)} \tag{4}$$

Suppose that R includes the base rules, then $R_{t+1} = R_t + r_t$ creates the new rule, and all base rules in R_{t+1} are summed; the sign of the sum defines the classification rule as follows:

$$\text{class}(x) = \text{sign} \left(\sum_{t=1}^T r_t(x) \right) \tag{5}$$

where T is the number of training instances, r_i is the two prediction values (a and b) at each layer of the tree, and x is a set of instances.

2.4. Naïve Bayes Tree

The naïve Bayes tree (NBTree) is a hybrid model that comprises the naïve Bayes and decision tree classifiers [86]. It replaces the leaf node of the built decision tree with a naïve Bayes classifier [87,88]. During the past few years, several researchers have shown great interest in the application of the NBTree algorithm in the field of classification and its satisfactory performance has been demonstrated [85–87,89]. The classification rule for naïve Bayes is defined as follows:

$$\begin{aligned} C^* &= \operatorname{argmax}_{c_j \in C} P(c_j | a_1, a_2, \dots, a_m) = \frac{P(c_j) \prod_{i=1}^m p(a_i | c_j)}{\sum_{j=1}^k \left[p(c_j) \prod_{i=1}^m p(a_i | c_j) \right]} \\ &= \mu \operatorname{argmax}_{c_j \in C} P(c_j) \prod_{i=1}^m p(a_i | c_j) \end{aligned} \quad (6)$$

where c_j is the output class of class set C , a_1, a_2, \dots, a_m are the conditionally independent factors, and k is the total number of classes.

2.5. Logistic Model Tree

Logistic model tree (LMT) was proposed by Landwehr, et al. [90] for classification purposes. This algorithm incorporates a decision tree and linear logistic regression in a single tree to increase prediction accuracy [90]. This has led to various applications of LMT in geoscience studies [62,91,92]. To use the capability of the two algorithms, LMT uses the LogitBoost algorithm to fit the logistic regression at the nodes of the tree [93]. For the fully-grown tree, LMT applies the CART algorithm [94] for pruning and a cross-validation technique is applied to select the optimal subtree [95]. The LogitBoost incrementally refines the logistic regression model by introducing least-squares fitting additive modeling; the probability of each leaf nodes in class M_i is calculated by simple logistic regression [95–97] as follows:

$$L_M(x) = \sum_{i=1}^n \beta_i x_i + \beta_0 \quad (7)$$

$$P(M|x) = \frac{\exp(L_M(x))}{\sum_{M'=1}^D \exp(L_{M'}(x))} \quad (8)$$

where n is the number of factors in vector x , β_i and β_0 are the coefficient and intercept of the regression, respectively, and D is the number of classes.

2.6. Artificial Neural Network

Artificial neural network (ANN) is a computational mechanism that has been developed as a crude attempted replication of the human brain [98]. An attractive feature of ANN is its approach that does not consider any particular hypothesis with respect to the statistical distribution of the information [78]. In contrast to classical statistical models, it can model non-linear relationships between predictor and target variables [99]. The significant abilities of ANNs, such as high learning ability, ability to work with high-dimensional data and generalization [100,101], have led to it being a widely used method for various types of prediction problems [102].

Among the different types of ANN structures, three structures, including the single-layer feed-forward ANN (SLFF-ANN), the multi-layer feed-forward ANN (MLFF-ANN), and the recurrent ANN are the most used structures, among which the MLFF-ANN is the most popular [103]. The MLFF-ANN consists of three layers, including an input layer, output layer and a hidden layer, which is located between the input and output layers [104].

At first, the network begins with multiplication of the random weights and data, which are fed into the input neuron. The resulting values are summed to calculate the input to the neurons in the next layer. Then, a non-linear activation function is used to convert the input value to the known output, as in Equation (9):

$$O_j = f(\text{net}) = f\left(\sum_{i=1}^n w_{ij}x_i + b_j\right) \quad (9)$$

where O_j is the calculated amount of the neuron j , f is the activation function, w_{ij} and b_j are the weight and bias of the j th neuron for i th input x .

Finding the appropriate connection weights is known as optimization of the network which is performed in the training step using various learning algorithms. The most widely used learning algorithm is the gradient descent algorithm incorporated with back propagation (BP). To minimize the error between the estimated output and observed value, the BP algorithm tries to find the optimized weights between the layers of the network [105,106]. After finding the weights with the least error, the network is called a trained network and will be evaluated with a new dataset to calculate its generalization capability [103].

2.7. Boosted Regression Trees

The boosted regression tree (BRT) technique is an advanced model that combines decision trees (weak learners) of fixed size and a robust boosting technique, as follows [107]:

$$F_m(x) = \sum_{m=1}^M \gamma_m h_m(x) \quad (10)$$

where $F_m(x)$ is the final model, γ_m is a learning rate, $h_m(x)$ are weak learners, and M is the number of iterations.

The boosting technique enhances the accuracy of the prediction by reducing the final model variance [108]. To do this, boosting interactively fits new trees to the residual errors of the existing tree to build a large ensemble of small regression trees to demonstrate the complex relationships between the target and predictor variables (Equation (11)) [109].

$$F_m(x) = F_{m-1}(x) + \gamma_m h_m(x) \quad (11)$$

Considering the loss function $L(y, F(x))$ and training dataset $D = \{(x_1, y_1), \dots, (x_n, y_n)\}$, at each step, weak learners $h_m(x)$ are used to minimize the loss function using the current model F_{m-1} and its fit $F_{m-1}(x_i)$:

$$F_m(x) = F_{m-1}(x) + \underset{h}{\operatorname{argmin}}(x) \sum_{i=1}^n L(y_i, F_{m-1}(x_i) - h_m(x)) \quad (12)$$

BRT uses a stochastic gradient boosting approach to solve this minimization problem:

$$F_m(x) = F_{m-1}(x) + \gamma_m \sum_{i=1}^n \nabla_F(y_i, F_{m-1}(x_i)) \quad (13)$$

The strong learning ability and flexibility of the BRT model in dealing with complex data have been proven by several studies in different fields, such as urban expansion [110], environmental science [111] and ecological modeling [112].

3. ML Methodology of GESM

To comprehensively review the state of the art of ML models for GESM, top peer-reviewed papers were chosen by implementing search engines, such as Scopus, ScienceDirect and the Web of Science (WOS) up to the present (2022). To select papers, the search

criteria were the terms ‘gully erosion’ and ‘machine learning’ and consideration of three types of quality measure, including the source-normalized impact per paper (SNIP), the cite score and the h-index. On this basis, 19 high-quality published papers were selected for the current review. Table 2 shows the detailed information for the selected papers.

Table 2. List of the reviewed publications, including the publisher’s name and journal characteristics.

Paper	Year	Publisher	Journal	SNIP	CiteScore	h-Index
[65]	2011	ScienceDirect	Geomorphology	1.504	7.3	171
[18]	2011	ScienceDirect	Computers & Geosciences	1.664	7	131
[113]	2014	ScienceDirect	Geomorphology	1.504	7.3	171
[114]	2016	ScienceDirect	Geomorphology	1.504	7.3	171
[98]	2017	ScienceDirect	Geomorphology	1.504	7.3	171
[115]	2019	ScienceDirect	Science of The Total Environment	2.175	14.1	275
[116]	2019	ScienceDirect	Physics and Chemistry of the Earth, Parts A/B/C	1.119	5.4	86
[69]	2019	ScienceDirect	Geoderma	2.048	11.1	177
[62]	2019	ScienceDirect	Geoscience Frontiers	2.549	11.8	65
[117]	2019	ScienceDirect	Science of The Total Environment	2.175	14.1	275
[118]	2019	ScienceDirect	Journal of Environmental Management	1.907	11.4	196
[72]	2020	ScienceDirect	Geoscience Frontiers	2.549	11.8	65
[119]	2020	ScienceDirect	Geomorphology	1.504	7.3	171
[120]	2021	Nature	Scientific Reports	4.54	7.1	242
[121]	2021	ScienceDirect	Geomorphology	1.504	7.3	171
[122]	2021	ScienceDirect	Ecological Informatics	1.436	5.4	60
[123]	2021	ScienceDirect	Alexandria Engineering Journal	2.102	8.3	68
[124]	2021	ScienceDirect	Geoscience Frontiers	2.549	11.8	65
[125]	2021	MDPI	ISPRS International Journal of Geo-Information	0.72	5	52

From the reviewed papers, typically, four main steps are used in ML-related GESM studies to obtain accurate results. These steps are (i) preparation of an inventory map of gullies, (ii) creation of gully conditioning factors, (iii) multi-collinearity assessment, and (iv) model development and performance evaluation. Each step is described and discussed below.

3.1. Inventory Map of Gullies

A gully erosion inventory map (GEIM) is created to provide the location and spatial distribution of the gullies in the study area [62]. Generally, for producing an inventory map, the gullies are determined with an extensive field survey using the global positioning system (GPS) and are validated with ancillary data, such as high-resolution images acquired from Google Earth [62,64,115]. After selecting the pixels that show gully erosion, the non-gully pixels, which are located in pixels other than the gully pixels, are selected and merged with gully erosion pixels to create a dataset of gully presence (positive cases) and absence (negative cases) for each set. The non-gully pixels are created randomly; it is recommended that the ratio of gully and non-gully pixels should be equal to one [98,126,127]. In the next step, the GEIM dataset is divided into two groups, the training and validation sets to be used for ML model development. In the literature, it is suggested that 70% of the dataset is used for model training, and that the other 30% is considered as a validation set [62,72,98,100,128]. Table 3 shows the detailed characteristics of the study area, the resolution of the imageries used, and the number of digitized gullies in each reviewed GESM study. As illustrated in the table, the number of digitized gullies is different in each study based on the attributes of the area. However, in most studies, the gully inventory has been split into training and test datasets based on the 70/30 rule.

Table 3. Characteristics of the study area, resolution of the imageries and information of GEIM used in GESM studies.

Paper	Location	Study Area Size	Study Area Climate	Spatial Resolution of the Data	Digitizing Method	GEIM Characteristics		
						Number of Digitized Gullies (Areas)	Train Set Number (Percentage)	Validation Set Number (Percentage)
[65]	Italy	42 km ²	Mediterranean	10 m	Not specified	Not specified	Not specified	Not specified
[18]	Turkey	424 km ²	Arid	25 m	Gully system areas	– (20)	9 (–)	11(–)
[113]	Morocco	390 km ²	Sub-humid to Semi-arid	15 m	Gully system areas	Not specified	Not specified	Not specified
[114]	Italy	9.5 km ²	Mediterranean	2 m	Individual gullies	260 (–)	–(75%)	–(25%)
[98]	Iran	245 km ²	Semi-arid	10 m	Individual gullies	65 (–)	45(70%)	20(30%)
[115]	Iran	18.5 km ²	Semi-arid	10 m	Individual gullies	Not specified	Not specified	Not specified
[116]	South Africa	59 Km ²	Subtropical	10 m	Individual gullies	83(–)	58 (70%)	25 (30%)
[69]	Iran	4274 km ²	Semi-arid	10 m	Individual gullies	207(–)	146(70%)	61(30%)
[62]	Iran	1329 km ²	Semi-arid	12.5 m	Individual gullies	303(–)	212(70%)	91(30%)
[117]	India	709 km ²	Monsoon	20 m	Individual gullies	174(–)	121(70%)	53(30%)
[118]	Iran	5757 km ²	Arid	12.5 m	Individual gullies	215(–)	150(70%)	65(30%)
[72]	Iran	3430 km ²	Semi-arid	30 m	Individual gullies	462(–)	323(70%)	139(30%)
[119]	Iran	2820 km ²	Arid to Semi-arid	30 m	Individual gullies	359(–)	251(70%)	107(30%)
[120]	Iran	505 km ²	Arid	12.5 m	Individual gullies	293(–)	206(70%)	87(30%)
[121]	India	442 km ²	Monsoon	12.5 m	Individual gullies	120(–)	84(70%)	36(30%)
[122]	India	357 km ²	Tropical monsoon	12.5 m, 30 m	Individual gullies	199(–)	139(70%)	60(30%)
[123]	Iran	75 km ²	Semi-arid	12.5 m	Individual gullies	103(–)	72(70%)	31(30%)
[124]	Iran	Not specified	Arid	12.5 m, 30 m	Individual gullies	Not specified	Not specified (70%)	Not specified (30%)
[125]	China	10.9 km ²	Semi-arid	1 m	Individual gullies	353(–)	247(70%)	106(30%)

3.2. Gully Conditioning Factors

The choice of appropriate geo-environmental factors (GEFs) is an important step for the construction of an accurate gully erosion susceptibility map [98,115,129]. A wide range of GEFs, such as primary topographic attributes (e.g., slope, elevation, slope degree, aspect) and secondary topographic attributes (e.g., stream power index, terrain ruggedness index, topographic wetness and position indices) that contribute to the spatial distribution of gullies has been employed by different researchers in the literature [1]. Table 4 presents a review of the different gully erosion studies with a focus on GEFs that have been used in each publication.

Table 4 shows that some GEFs, such as primary and secondary topographic attributes are the most used factors in GESM. On the other hand, some factors (e.g., convergence index, terrain ruggedness index, topographical position index) have not been used in most studies. This means that a standard methodology has not yet been accepted by scientists as a globally accepted procedure for the selection of GEFs [130]. However, some authors have tried to investigate the importance of different GEFs to identify the most effective GEFs that significantly affect the accuracy of GESM. For example, Akgün and Türk [18] in their study for GESM in the Ayvalık region, located northwest of Turkey, investigated the importance of different GEFs for erosion susceptibility. Among seven GEFs considered, the weathering grades of rocks, lineament density and drainage density were the most effective factors for erosion, while slope gradient and land cover achieved a second importance ranking.

Soil surface properties represent another set of factors that significantly affect the quality of GESM due to their influence on resistance to erosion, infiltration and runoff rate [131,132]. Thus, soil texture has attracted much attention from different researchers in the investigation of gully erosion susceptibility [98,129,133–138]. In addition to soil texture, Garosi, Sheklabadi, Conoscenti, Pourghasemi and Van Oost [115] used two other soil properties, soil organic carbon (SOC) and calcium carbonate equivalent (CCE), as predictor variables for GESM, in addition to other controlling factors. A variable importance analysis showed that three GEFs factors, including distance from rivers, CCE, and the topographic position index (TPI), significantly affected the accuracy of GESM. Roy and Saha [121] also found that the soil type factor had the most marked effect on GESM.

In another study, Amiri, Pourghasemi, Ghanbarian and Afzali [69] concluded that, among all the applied factors, three factors, including distance from the river, clay percent, and land use, noticeably affected GESM. Results obtained by Arabameri, Chen, Loche, Zhao, Li, Lombardo, Cerda, Pradhan and Bui [62] showed that, among eighteen GEF factors, drainage density, rainfall and slope were the most effective factors for predicting gully occurrences. A variable importance analysis conducted by Pourghasemi, Sadhasivam, Kariminejad and Collins [72] showed that the distance from rivers and the plan curvature had the most and the least importance, respectively, with respect to finding the zones most prone to gullying.

It is common in the field of GESM that a variable identified as the most important factor in one study is not found to be important in another study. For example, a variable importance analysis conducted by Pourghasemi, Sadhasivam, Kariminejad and Collins [72] showed that slope had the highest effect on gully erosion, but Gayen, Pourghasemi, Saha, Keesstra and Bai [117], in their study, concluded that slope had the lowest importance. As suggested by Gutiérrez, et al. [139] and Garosi, Sheklabadi, Conoscenti, Pourghasemi and Van Oost [115], this could be because some variables do not contribute to the spatial distribution of gullies, because there are some uncertainties related to the accurate quantification of these variables, or because there is significant variation in the effect of variables in different environments. However, most studies have suggested that the primary topographic attributes (e.g., elevation, slope and plan curvature), hydrological properties, such as rainfall, and anthropogenic factors, such as land use/cover are among the most important factors that significantly affect the quality of GESM [72,98,117,118].

Table 4. List of most widely used GEFs in different ML-based publications for GESM.

Paper	Primary Topographic Attributes								Secondary Topographic Attributes				Hydrological Properties				Anthropogenic Factors		Soil Surface Properties				Other Factors							
	Elevation	Slope aspect	Slope degree	Slope length	Catchment area	Curvature	Plan curvature	Profile curvature	Convergence index	Stream power index	Terrain ruggedness index	Topographic wetness index	Topographic position index	Terrain surface texture	Rainfall	Drainage density	Distance to streams	Transport capacity index	Distance to road	Land Use/Cover	Soil texture	Soil organic carbon	Calcium carbonate equivalent	Iron Oxid	Remote sensing indices (NDVI)	Lithology	Lineament density	Fractional vegetation cover	Distribution of terrace	
[65]	*	*	*				*	*	*		*					*	*													
[18]			*					*	*							*	*												*	
[113]	*	*		*	*		*	*	*	*															*					
[114]	*	*	*	*			*	*	*	*							*	*			*					*				
[98]	*	*	*				*	*	*		*					*	*		*	*	*				*	*	*	*	*	
[115]	*	*	*		*		*	*	*	*		*					*	*	*	*	*	*	*	*	*	*	*	*	*	
[116]			*				*	*	*	*							*	*			*	*	*	*	*	*	*	*	*	
[69]	*	*	*				*	*	*	*				*	*	*	*		*	*	*			*	*	*	*	*	*	
[62]	*	*	*		*		*	*	*	*	*	*	*	*	*	*	*	*	*	*	*	*	*	*	*	*	*	*	*	
[117]	*	*	*				*	*	*	*						*	*	*	*	*	*	*	*	*	*	*	*	*	*	
[118]	*	*	*				*	*	*	*				*	*	*	*	*	*	*	*	*	*	*	*	*	*	*	*	
[72]	*	*	*				*	*	*	*				*	*	*	*	*	*	*	*	*	*	*	*	*	*	*	*	
[119]	*	*	*	*			*	*	*	*				*	*	*	*	*	*	*	*	*	*	*	*	*	*	*	*	
[120]	*		*				*	*	*	*	*	*	*	*	*	*	*	*	*	*	*	*	*	*	*	*	*	*	*	
[121]	*	*	*				*	*	*	*	*	*	*	*	*	*	*	*	*	*	*	*	*	*	*	*	*	*	*	
[122]	*	*	*				*	*	*	*	*	*	*	*	*	*	*	*	*	*	*	*	*	*	*	*	*	*	*	
[123]	*	*	*				*	*	*	*	*	*	*	*	*	*	*	*	*	*	*	*	*	*	*	*	*	*	*	
[124]	*	*	*				*	*	*	*	*	*	*	*	*	*	*	*	*	*	*	*	*	*	*	*	*	*	*	
[125]	*	*	*	*	*	*			*	*	*	*	*	*	*	*	*	*	*	*	*	*	*	*	*	*	*	*	*	*

For a detailed description of the GEF factors, see Garosi, Sheklabadi, Conoscenti, Pourghasemi and Van Oost [115] and Arabameri, Chen, Loche, Zhao, Li, Lombardo, Cerda, Pradhan and Bui [62].

The spatial resolution of the GEFs is the most important factor that significantly affects the accuracy of GESM. As can be seen in Table 3, different spatial resolutions from 1 m to 30 m have been used in different studies to derive GEFs. However, choosing the proper spatial resolution of imageries for the extraction of GEFs depends on the extent of the study area and the availability of the data, and only a few studies have sought to assess the effect of the spatial resolution on the accuracy of the ML models developed on the same study area. For example, Chowdhuri, Pal, Saha, Chakraborty and Roy [122] compared five types of DEM, i.e., shuttle radar topography mission (SRTM), advanced spaceborne thermal emission and reflection radiometer (ASTER), Cartosat-1, advanced land-observing satellite (ALOS) World 3D-30 m (AW3D30) with a spatial resolution of 30 m, and ALOS PALSAR with a spatial resolution of 12.5 m, to evaluate the scale-dependence of DEM-derived GEFs in GESM. The results obtained showed that the developed models with ALOS PALSAR produced higher accuracy than the developed models with other types of DEM. The results also showed that, although the DEMs with 30 m spatial resolution produced comparable results, of these, the AW3D30 produced the most appropriate results. In a similar study, Arabameri, Rezaie, Pal, Cerda, Saha, Chakraborty and Lee [124] compared the predictive ability of GEFs derived from three types of DEM (i.e., ALOS PALSAR = 12.5 m, AW3D30 and ASTER = 30 m). The results showed that the ML models developed by GEFs derived from ALOS PALSAR produced the most appropriate results followed by the models developed by AW3D30 and ASTER.

Although the results of the studies described have demonstrated the superiority of the developed ML models with finer resolution images, the results of studies conducted by Gayen, Pourghasemi, Saha, Keesstra and Bai [117], Akgün and Türk [18], and Pourghasemi, Sadhasivam, Kariminejad and Collins [72] showed that ML models developed with coarser spatial resolution data (e.g., 20, 25 and 30 m) can provide satisfactory results for gully detection. Among the papers reviewed, only two papers used high resolution images for the preparation of GEFs. Angileri, Conoscenti, Hochschild, Märker, Rotigliano and Agnesi [114], in their study, used a DEM with 2 m spatial resolution to produce a gully erosion susceptibility map in a river catchment with an area of 9.5 km². In another study, Yang, Wang, Pang, Long, Wang, Cruse and Yang [125] used 1 m digital surface models obtained by UAV to produce a gully erosion susceptibility map in a small watershed with an area of 10.9 km². Although both studies obtained good predictive performance for the ML models, the applied high-resolution imageries in these studies cannot easily be used in large areas because of the difficulties associated with the acquisition of the high-resolution data and the computation costs. Therefore, the application of these types of data is limited to small areas.

3.3. Multi-Collinearity Assessment

Due to the large number of built GEFs in GESM, multi-collinearity problems occur that can lead to a reduction in model accuracy. The multi-collinearity issue arises when several factors are strongly correlated, which can lead to mistakes and misinterpretation in the model estimations [137,140]. Therefore, a multi-collinearity evaluation is considered an essential step after preparing the GEFs [72,115]. Generally, two statistical indicators, namely, the tolerance (TOL) and the variance inflation factor (VIF) are utilized to calculate the multi-collinearity of variables. These two indicators are defined in Equations (14) and (15):

$$\text{TOL} = 1 - R_i^2 \quad (14)$$

$$\text{VIF} = \frac{1}{1 - R_i^2} \quad (15)$$

where R_i^2 is the coefficient of determination, calculated for the i th variable (e.g., x_1, \dots, x_n) against every other variable in the model. Bui, et al. [141] suggested that a $\text{TOL} < 0.1$ and a $\text{VIF} > 10$ indicate a multi-collinearity problem.

3.4. Model Development and Performance Evaluation

In this step, all ML models are trained using a training set to find the optimum parameters of each model that produce the best results for detection of the gully and non-gully pixels in the training set and then the trained models are tested on the validation set. Validation of the developed models is an important task for the evaluation of the predicted gully erosion susceptibility maps (GESMs) [18]. The validation process includes goodness of fit and predictive accuracy steps, whereby the former is used for model evaluation in the training dataset and the latter computes the model performance in predicting a validation dataset [141]. Typically, two types of performance measures, including threshold-dependent and threshold-independent methods, are used for validation of the predicated GESMs in related studies [98]. In most studies, three indicators are employed to assess the model performance: accuracy and Kappa coefficients for the threshold-dependent methods, and the receiver operating characteristic (ROC) curve for the threshold-independent method.

3.4.1. Accuracy

To compute the accuracy, predicted gully susceptibility maps are divided into gully or non-gully classes. Then, a contingency matrix (Table 5) is applied that has four components: true positive (TP) and true negative (TN), which show the total number of gully occurrence and non-gully occurrence pixels that are correctly classified, false positive (FP) that shows the number of non-gully pixels that are misclassified and incorrectly considered as gully pixels, and false negative (FN) that shows the number of gully pixels which are incorrectly detected as non-gully pixels.

$$\text{Accuracy} = \frac{\text{TP} + \text{TN}}{\text{TP} + \text{TN} + \text{FP} + \text{FN}} \tag{16}$$

Table 5. Contingency matrix employed for calculation of accuracy and Kappa coefficients.

Observed	Predicted	
	Non-Gully (−)	Gully (+)
Non-gully (−)	(− −) True negative (TN)	(+ −) False positive (FP)
Gully (+)	(− +) False negative (FN)	(+ +) True positive (TP)

3.4.2. Kappa Coefficient

The Kappa coefficient (Equation (17)) demonstrates the ability of the models for classification based on the proportion of the observed agreements (P_o) and the hypothetical probability of expected agreements (P_e), which account for the occurrences that happened by chance [142].

$$\text{Kappa} = \frac{P_o - P_e}{1 - P_e} \tag{17}$$

P_o and P_e can be defined as in Equations (18) and (19):

$$P_o = \frac{\text{TP} + \text{TN}}{\text{TN} + \text{TP} + \text{FP} + \text{FN}} \tag{18}$$

$$P_e = \frac{\left(\frac{(\text{TN} + \text{FN}) * (\text{TN} + \text{FP})}{\text{TN} + \text{TP} + \text{FP} + \text{FN}} \right) + \left(\frac{(\text{TP} + \text{FP}) * (\text{TP} + \text{FN})}{\text{TN} + \text{TP} + \text{FP} + \text{FN}} \right)}{\text{TN} + \text{TP} + \text{FP} + \text{FN}} \tag{19}$$

Landis and Koch [143] categorized the model performance based on the Kappa coefficient into six groups: ≤ 0 (poor), 0–0.2 (slight), 0.2–0.4 (fair), 0.4–0.6 (moderate), 0.6–0.8 (substantial) and 0.8–1 (almost perfect).

3.4.3. Receiver Operating Characteristic (ROC) Curve

The ROC curve is a well-known technique for quantitatively describing the efficiency of probabilistic tests [144,145]. To obtain ROC, two vectors are required, where one vector indicates the binary condition of the presence-absence of a given problem and the other demonstrates the corresponding probability estimates [89,146]. The shape of the ROC curve can be used to assess the ability of the model for prediction, where the higher performance is near the upper left part of the curve [18]. In addition to the shape, the accuracy can be computed using the area under the ROC curve (AUC), which has been widely applied as a measure to quantify the performance of predictive models [147]. According to the literature [147,148], AUC values for the accuracy assessment of models can be classified as follows: poor (0.5–0.6), moderate (0.6–0.7), good (0.7–0.8), very good (0.8–0.9) and excellent (0.9–1.0).

3.5. Software and Programming Languages Used for GESM

To accomplish the aims of the GESM using the four main steps described above, different software programs and programming languages are used by researchers, as follows:

1. ArcGIS and SAGA-GIS software are typically implemented for preprocessing steps, such as preparing the inventory map of gullies and GEFs.
2. MATLAB, Python, and R programming languages are used for multi-collinearity assessment, ML model development and performance evaluation.

4. Comparative Performance Analysis of ML

In this section, the predictive ability of ML models used in the studies reviewed is compared and discussed to identify the models that are the most appropriate for GESM. Some researchers have highlighted the suitability of certain ML techniques, such as support vector machine (SVM), artificial neural network (ANN), random forest (RF), decision tree (DT), and boosted regression tree (BRT), for gully erosion studies [64,114,149–151].

Märker, Pelacani and Schröder [65] compared RF with stochastic gradient boosting (TreeNet: TN) to produce susceptibility maps (rill-interrill erosion and gullies) for the Orme River, Italy. The comparison of the models using AUC, the Kappa coefficient, and pseudo R^2 showed that, although both models provided good accuracy, TN outperformed RF. However, TN showed instability between the training and validation accuracy that occurred due to overfitting. In contrast, RF was more stable during the training and validation phases. Rahmati, Tahmasebipour, Haghizadeh, Pourghasemi and Feizizadeh [98], in a study that was carried out in the Kashkan–Poldokhtar Watershed, Iran, compared seven ML models, including SVM, with four well-known kernel types (radial basis function, polynomial, linear and sigmoid), RF, ANN, and BRT for GESM. All the applied models were tested on three different sample sets to comprehensively assess the performance of each model. To produce the GESMs, 12 GEFs were employed as predictors. It was concluded that the accuracy ranking was RF > SVM-RBF > BRT > SVM-polynomial. The RF and SVM-RBF showed the most predictive accuracy for GESM. The superiority of RF over other models has also been reported by other researchers [69,72,115,117] (Table 6). The excellent prediction performance of RF for gully detection is accounted for by the following: (1) RF is capable of using all predictors with different types without removing any parameter during the modeling; (2) RF can work with very large datasets; (3) since RF can create multiple predictions of each phenomenon using a combination of trees, it can find the non-linear relationships between predictors and predictands; (4) RF combines different types of data in the analysis to overcome the problems associated with lack of distribution of assumptions related to the input data; and (5) RF shows less sensitivity to the noise in data [152–154].

Table 6. List of recent studies in the area of GESM using ML techniques.

Paper	Evaluation Criteria	Results
[65]	AUC, Kappa, R ²	TreeNet: TN > RF; RF was more stable
[18]	AUC	Logistic regression is accurate
[113]	User’s and producer’s accuracy	RF is useful
[114]	AUC	SGT is outstanding
[98]	AUC, Kappa, accuracy	RF > SVM-RBF > BRT > SVM-polynomial > ANN
[115]	AUC, Kappa, accuracy, RMSE, MAE	RF > SVM > NB > GAM
[116]	User’s and producer’s accuracy	SVM is useful
[69]	AUC	RF > SVM > BRT
[62]	AUC	LMT > NBTree > ADTree
[117]	AUC	RF > MARS > SVM > FDA
[118]	AUC, SCAI ^a , FR ^b	GWR-CF-RF > CF-RF > RF > CF
[72]	AUC	RF outperformed the other 9 models
[119]	AUC, accuracy, TSS ^c	DS-BL > DS-RLG > DS-RL > DS-BLW > DS
[120]	AUC, Kappa, RMSE, F-score, accuracy	CDT-RF > CDT-ADTree > CDT-BA > CDT-DA > CDT
[121]	AUC, MAE, RMSE	MLP-Dagging > MLP-Bagging > MPL
[122]	Sensitivity, specificity, accuracy, precision, F-score, Kappa and AUC	DLNN > CNN > ANN
[123]	Sensitivity, specificity, positive predictive value (PPV), negative predictive value (NPV), and AUC	OB RF > OB BRT > OB SVM
[124]	Accuracy, sensitivity, specificity, Kappa coefficient, and AUC	Cforest > elastic net > cubist
[125]	AUC	XGBoost > RF > GBDT

(a) SCAI is the ratio of the surface area of the class to the gully surface area of that class. (b) FR is the ratio of the gully surface area in each class to the surface area of that class. (c) TSS is the true skill statistic.

For these reasons, RF has received significant attention in gully erosion studies. For example, Shruthi, Kerle, Jetten and Stein [113], in their study for gully system prediction using object-oriented analysis and ASTER data, employed an RF technique to find the relationship between the explanatory variables and gully erosion. Their results showed that satellite images with medium resolution had enough information for GESM based on an overall performance of 81% (OOB error of 19%). Kuhnert, Henderson, Bartley and Herr [151] proposed a methodology for the assessment of errors associated with gully density mapping in the Burdekin catchment in Queensland, Australia, using an RF modeling approach.

Among all the applied models for GESM, after RF, SVM is the second most used method in gully erosion studies and its ability has been demonstrated by different researchers. For example, results obtained by Rahmati, Tahmasebipour, Haghizadeh, Pourghasemi and Feizizadeh [98], Garosi, Sheklabadi, Conoscenti, Pourghasemi and Van Oost [115], and Amiri, Pourghasemi, Ghanbarian and Afzali [69], showed that SVM achieved the second ranking after RF for GESM. The good performance of SVM is related to its ability to analyze non-linear relationships [155] and also because it is less sensitive to the input data, which makes SVM a powerful tool for the detection of a wide range of geo-environmental problems [156–158]. Therefore, this model has also been used by researchers for gully erosion mapping. Makaya, Mutanga, Kiala, Dube and Seutloali [116] assessed the applicability of a Sentinel-2 MSI multispectral sensor for GESM in the Okhombe Valley, South Africa. The SVM model was applied for gully classification, and the accuracy of the model was assessed using a confusion matrix. The results showed that SVM achieved an overall classification accuracy of 77% for GESM.

In addition to the RF and SVM, other ML models, such as logistic regression [18]; stochastic gradient treeboost [114], the logistic model tree (LMT), the alternating decision tree (ADTree), the naïve Bayes tree (NBTree) [62], deep learning neural network (DLNN) [122], conditional inference forests (Cforest) [124], and extreme gradient boosting (XGBoost) [125], have shown high predicative accuracy for GESM (Table 6).

Comparison of published papers in the field of GESM using ML techniques shows that several developments have occurred in ML applications from 2011 to 2021 (Table 2).

For example, recent studies have attempted to develop novel/hybrid models to produce better predictive performance than the ML techniques that are currently used for GESM. Arabameri, Pradhan and Rezaei [118] combined three methods, including the geographically weighted regression (GWR) technique, the certainty factor (CF) and random forest, (RF) to generate GESMs. The results showed that use of the GWR-CF-RF model resulted in better accuracy than the individual CF and RF models. In another study, a GIS-based hybrid model was proposed by Arabameri, Cerda, Pradhan, Tiefenbacher, Lombardo and Bui [119] for GESM. The Dempster–Shafer (DS) statistical model was combined with four kernels of BRT, including binary logistic, reg logistic, binary logitraw, and reg linear to create four hybrid models, including DS-binary logistic (DS-BL), DS-reg logistic (DS-RLG), DS-reg linear (DS-RL), and DS-binary logitraw (DS-BLW). Their results showed that the integration of the models increased prediction accuracy and DS-BL outperformed the other hybrid models. The individual DS model exhibited the worst performance among all the applied models.

In another study, Arabameri, Sadhasivam, Turabieh, Mafarja, Rezaie, Pal and Santosh [120] introduced novel hybrid ensemble models to detect gully-prone areas in the Bastam plain, Iran. Four new ensemble techniques, including credal decision tree-dagging (CDT-DA), credal decision tree-bagging (CDT-BA), credal decision tree-alternative decision tree (CDT-ADTree), and credal decision tree rotation forest (CDT-RF) were evaluated for GESM and compared with the results for an individual CDT. The results showed that use of CDT-RF resulted in greater accuracy than the other applied models.

Roy and Saha [121] evaluated gully erosion susceptibility in the Hinglo river basin, India, by utilizing the multilayer perceptron neural network (MLP) as the base classifier and two hybrid ensemble ML techniques, including bagging and dagging. Therefore, three models, including MLP, MLP-bagging, and MLP-dagging were developed and tested. The results of the accuracy assessment by AUC, MAE, and RMSE showed that MLP-bagging performed better than the other models.

Although many studies have been carried out in the field of GESM using ML techniques, researchers still contest the choice of the most accurate model because, in addition to the quality of the user data, the selection of the best model relies on the model structure [63]. For example, Märker, Pelacani and Schröder [65], in their study, concluded that the TreeNet model gives better results than RF, but Pourghasemi, Sadhasivam, Kariminejad and Collins [72] compared RF with nine ML methods with the results showing that RF outperformed the other models. Therefore, it is difficult to provide a ranking of ML models for GESM and more attention needs to be paid to comparison of the different ML techniques to draw reasonable conclusions and gain insights into the drawbacks and advantages of the techniques.

5. Conclusions and Recommendations

Gully erosion is an important problem that has a great impact on agricultural activities and economics by promoting land and water degradation. ML techniques have been applied in GESM to produce valuable tools for regional managers via identification of locations where gullies occur, as well as those that are susceptible to gully initiation, to assess the environmental impacts of gullies and plan gully erosion controls to mitigate its negative environmental effects. This paper presented a review of ML models employed in the field of GESM. To produce reliable gully erosion maps using ML techniques, four main steps are typically used: (i) producing inventory maps of gullies, (ii) extracting gully conditioning factors, (iii) multi-collinearity assessment, and (iv) model development and performance evaluation. With respect to GEFs, most studies have suggested that primary topographical attributes (e.g., elevation, slope and plan curvature), hydrological properties, such as rainfall, and anthropogenic factors, such as land use/cover, are among the factors that particularly affect the quality of GESM. The spatial resolution of GEFs is an important attribute of GEFs and different studies indicate that a spatial resolution of 1 m to 30 m can be used for GESM. However, the most suitable spatial resolution should be selected based

on different criteria, such as the objectives of the study, the extent of the study area, the availability of data, and computational resources. As shown in the present paper, there are many ML models used to estimate gully erosion susceptibility, some are more widely used (e.g., RF and SVM), and some are often used (e.g., logistic regression, ANN, NBTree). The two methods that have generally been found to be the best methods for gully erosion mapping are RF and SVM. Nonetheless, each method yields different results in different areas, and the selection of the best method greatly depends on the reliability of the training data. Therefore, further investigation is required to compare their capabilities for various regions that have different environmental conditions. Comprehensive validation of the applied models is another important step, for which, according to the literature, two types of performance measure are mostly used: threshold-dependent methods, such as accuracy and the Kappa coefficient, and threshold-independent methods, such as ROC.

Despite the promising results for the ML models in GESM, some suggestions to improve the quality of gully erosion susceptibility assessment prediction by ML models can be proposed. First, it is recommended to conduct further studies to test various factors (e.g., topographic and hydrologic) in different geospatial locations that may influence the accuracy of ML models. Second, data-mining models should be used to improve the quality of datasets based on a comprehensive analysis of the relationship between historical gully occurrence and causative factors. Third, an ensemble of models should be implemented to combine the ability of the models to increase the accuracy and decrease the uncertainty of the prediction.

Among the reviewed papers, besides mapping the prone areas to permanent gully erosion, some studies sought to use ML techniques for rill–interill erosion mapping [65,114] and ephemeral gully mapping [115]. Since rill–interill and ephemeral gully erosion are other important types of soil erosion, more studies are required to explore the ability of ML methods to predict these types of erosion to gain insights into the relationships between these erosion processes and their controlling factors.

Considering the published papers in GESM using ML techniques, although the GESMs can be used as a valuable tool for the detection of degraded lands by gully erosion, the maps produced cannot reliably identify the gully trajectories which are the main input of some process-based models (e.g., CREAMS) for quantifying the soil loss from gullies. Therefore, it is recommended to combine topographic indices and ML models to provide more accurate estimation of gully trajectories that can be used in process-based models for the estimation of soil loss from gullies. With the help of ML models that can consider the combined effect of different GEFs on gully development, maps which show the spatial distribution of gully erosion occurrence can be produced. Topographic indices can use these distribution maps to extract gully trajectories based on topographic attributes.

Author Contributions: H.M.: writing—original draft preparation; A.B., R.R. and P.D.: review and editing. All authors have read and agreed to the published version of the manuscript.

Funding: Funding for this study was provided from a Natural Sciences and Engineering Research Council of Canada (NSERC) grant and the Ontario Ministry of Agriculture, Food and Rural Affairs (OMAFRA) Agrifood Alliance, grant number RGPIN-2017-04400.

Data Availability Statement: Not applicable.

Conflicts of Interest: The authors declare no conflict of interest.

References

1. Valentin, C.; Poesen, J.; Li, Y. Gully erosion: Impacts, factors and control. *Catena* **2005**, *63*, 132–153. [[CrossRef](#)]
2. Boardman, J.; Parsons, A.; Holland, R.; Holmes, P.; Washington, R. Development of badlands and gullies in the Sneeuberg, Great Karoo, South Africa. *Catena* **2003**, *50*, 165–184. [[CrossRef](#)]
3. Foster, G. Understanding ephemeral gully erosion. *Soil Conserv.* **1986**, *2*, 90–125.
4. Soil Science Society of America. *Glossary of Soil Science Terms*; Soil Science Society of America: Washington, DC, USA, 2001.
5. Poesen, J. Contribution of gully erosion to sediment production. In *Proceedings of the Erosion and Sediment Yield: Global and Regional Perspectives: Proceedings of an International Symposium, Exeter, UK, 15–19 July 1996*; p. 251.

6. Stout, B. Soil erosion by water, some measures for its control on cultivated lands. In *FAO Agricultural Development Economics Working Paper*; FAO: Roma, Italy, 1965.
7. U.S.C. Service. Procedure for determining rates of land damage, land depreciation and volume of sediment produced by gully erosion. *Guidel. Watershed Manag.* **1977**, *1*, 125–141.
8. Poesen, J.; Nachtergaele, J.; Verstraeten, G.; Valentin, C. Gully erosion and environmental change: Importance and research needs. *Catena* **2003**, *50*, 91–133. [[CrossRef](#)]
9. Chaplot, V.; Le Brozec, E.C.; Silvera, N.; Valentin, C. Spatial and temporal assessment of linear erosion in catchments under sloping lands of northern Laos. *Catena* **2005**, *63*, 167–184. [[CrossRef](#)]
10. Zucca, C.; Canu, A.; Della Peruta, R. Effects of land use and landscape on spatial distribution and morphological features of gullies in an agropastoral area in Sardinia (Italy). *Catena* **2006**, *68*, 87–95. [[CrossRef](#)]
11. Gomez Gutierrez, A.; Schnabel, S.; Felicísimo, A.M. Modelling the occurrence of gullies in rangelands of southwest Spain. *Earth Surf. Process. Landf. J. Br. Geomorphol. Res. Group* **2009**, *34*, 1894–1902. [[CrossRef](#)]
12. Popp, J.H.; Hyatt, D.E.; Hoag, D. Modeling environmental condition with indices: A case study of sustainability and soil resources. *Ecol. Model.* **2000**, *130*, 131–143. [[CrossRef](#)]
13. Sidorchuk, A.; Märker, M.; Moretti, S.; Rodolfi, G. Gully erosion modelling and landscape response in the Mbuluzi River catchment of Swaziland. *Catena* **2003**, *50*, 507–525. [[CrossRef](#)]
14. Conoscenti, C.; Angileri, S.; Cappadonia, C.; Rotigliano, E.; Agnesi, V.; Märker, M. Gully erosion susceptibility assessment by means of GIS-based logistic regression: A case of Sicily (Italy). *Geomorphology* **2014**, *204*, 399–411. [[CrossRef](#)]
15. Kumar, B. Carbon sequestration potential of tropical homegardens. In *Tropical Homegardens*; Springer: Berlin/Heidelberg, Germany, 2006; pp. 185–204.
16. Daggupati, P.; Sheshukov, A.Y.; Douglas-Mankin, K.R. Evaluating ephemeral gullies with a process-based topographic index model. *Catena* **2014**, *113*, 177–186. [[CrossRef](#)]
17. Wu, T.; Pan, C.; Li, C.; Luo, M.; Wang, X. A field investigation on ephemeral gully erosion processes under different upslope inflow and sediment conditions. *J. Hydrol.* **2019**, *572*, 517–527. [[CrossRef](#)]
18. Akgün, A.; Türk, N. Mapping erosion susceptibility by a multivariate statistical method: A case study from the Ayvalik region, NW Turkey. *Comput. Geosci.* **2011**, *37*, 1515–1524. [[CrossRef](#)]
19. Conoscenti, C.; Agnesi, V.; Cama, M.; Caraballo-Arias, N.A.; Rotigliano, E. Assessment of gully erosion susceptibility using multivariate adaptive regression splines and accounting for terrain connectivity. *Land Degrad. Dev.* **2018**, *29*, 724–736. [[CrossRef](#)]
20. Knisel, W.G. *CREAMS: A Field Scale Model for Chemicals, Runoff, and Erosion from Agricultural Management Systems*; US Department of Agriculture, Science and Education Administration: Washington, DC, USA, 1980.
21. Merkel, W.; Woodward, D.; Clarke, C. *Ephemeral Gully Erosion Model (EGEM)*; Woodward, Inc.: Fort Collins, CO, USA, 1988.
22. Leonard, R.; Knisel, W.; Still, D. GLEAMS: Groundwater loading effects of agricultural management systems. *Trans. ASAE* **1987**, *30*, 1403–1418. [[CrossRef](#)]
23. Sidorchuk, A. Dynamic and static models of gully erosion. *Catena* **1999**, *37*, 401–414. [[CrossRef](#)]
24. Gordon, L.; Bennett, S.; Bingner, R.; Theurer, F.; Alonso, C. Simulating ephemeral gully erosion in AnnAGNPS. *Trans. ASABE* **2007**, *50*, 857–866. [[CrossRef](#)]
25. Nearing, M.A.; Foster, G.R.; Lane, L.; Finkner, S. A process-based soil erosion model for USDA-Water Erosion Prediction Project technology. *Trans. ASAE* **1989**, *32*, 1587–1593. [[CrossRef](#)]
26. Bingner, R.L.; Theurer, F.D.; Yuan, Y. *AnnAGNPS Technical Processes*; USDA-ARS National Sedimentation Laboratory: Oxford, MS, USA, 2003.
27. Moore, I.; Burch, G.; Mackenzie, D. Topographic effects on the distribution of surface soil water and the location of ephemeral gullies. *Trans. ASAE* **1988**, *31*, 1098–1107. [[CrossRef](#)]
28. Thorne, C.; Zevenbergen, L.W.; Grissinger, E.; Murphey, J. Ephemeral gullies as sources of sediment. In Proceedings of the Fourth Federal Interagency Sedimentation Conference, Las Vegas, Nevada, 24–27 March 1986.
29. Beven, K.J.; Kirkby, M.J. A physically based, variable contributing area model of basin hydrology/Un modèle à base physique de zone d'appel variable de l'hydrologie du bassin versant. *Hydrol. Sci. J.* **1979**, *24*, 43–69. [[CrossRef](#)]
30. Wilson, J.P.; Gallant, J.C. *Terrain Analysis: Principles and Applications*; John Wiley & Sons: New York, NY, USA, 2000.
31. Douglas-Mankin, K.R.; Roy, S.K.; Sheshukov, A.Y.; Biswas, A.; Gharabaghi, B.; Binns, A.; Rudra, R.; Shrestha, N.K.; Daggupati, P. A comprehensive review of ephemeral gully erosion models. *Catena* **2020**, *195*, 104901. [[CrossRef](#)]
32. Vandekerckhove, L.; Poesen, J.; Wijdenes, D.O.; De Figueiredo, T. Topographical thresholds for ephemeral gully initiation in intensively cultivated areas of the Mediterranean. *Catena* **1998**, *33*, 271–292. [[CrossRef](#)]
33. Sekaluvu, L.; Sheshukov, A.Y.; Hutchinson, S.L. Accuracy of topographic index models at prediction of ephemeral gullies. In Proceedings of the 2015 ASABE Annual International Meeting, Chicago, IL, USA, 3–5 May 2015; p. 1.
34. Kumar, A.; Dwivedi, R.; Tiwari, K. The effects of image scale on delineation of eroded lands using remote sensing data. *Int. J. Remote Sens.* **1996**, *17*, 2135–2143. [[CrossRef](#)]
35. Zinck, J.A.; López, J.; Metternicht, G.I.; Shrestha, D.P.; Vázquez-Selem, L. Mapping and modelling mass movements and gullies in mountainous areas using remote sensing and GIS techniques. *Int. J. Appl. Earth Obs. Geoinf.* **2001**, *3*, 43–53. [[CrossRef](#)]
36. Manyatsi, A.M.; Ntshangase, N. Mapping of soil erosion using remotely sensed data in Zombodze South, Swaziland. *Phys. Chem. Earth Parts A/B/C* **2008**, *33*, 800–806. [[CrossRef](#)]

37. Liberti, M.; Simoniello, T.; Carone, M.; Coppola, R.; D'Emilio, M.; Macchiato, M. Mapping badland areas using LANDSAT TM/ETM satellite imagery and morphological data. *Geomorphology* **2009**, *106*, 333–343. [[CrossRef](#)]
38. Seutloali, K.E.; Beckedahl, H.R.; Dube, T.; Sibanda, M. An assessment of gully erosion along major armoured roads in south-eastern region of South Africa: A remote sensing and GIS approach. *Geocarto Int.* **2016**, *31*, 225–239. [[CrossRef](#)]
39. Phinzi, K.; Ngetar, N.S. Mapping soil erosion in a quaternary catchment in Eastern Cape using geographic information system and remote sensing. *South Afr. J. Geomat.* **2017**, *6*, 11–29. [[CrossRef](#)]
40. Daggupati, P.; Douglas-Mankin, K.R.; Sheshukov, A.Y. Predicting ephemeral gully location and length using topographic index models. *Trans. ASABE* **2013**, *56*, 1427–1440.
41. Sheshukov, A.Y.; Sekaluvu, L.; Hutchinson, S.L. Accuracy of topographic index models at identifying ephemeral gully trajectories on agricultural fields. *Geomorphology* **2018**, *306*, 224–234. [[CrossRef](#)]
42. Li, H.; Cruse, R.M.; Bingner, R.L.; Gesch, K.R.; Zhang, X. Evaluating ephemeral gully erosion impact on *Zea mays* L. yield and economics using AnnAGNPS. *Soil Tillage Res.* **2016**, *155*, 157–165. [[CrossRef](#)]
43. Wang, R.; Zhang, S.; Pu, L.; Yang, J.; Yang, C.; Chen, J.; Guan, C.; Wang, Q.; Chen, D.; Fu, B. Gully erosion mapping and monitoring at multiple scales based on multi-source remote sensing data of the Sancha River Catchment, Northeast China. *ISPRS Int. J. Geo-Inf.* **2016**, *5*, 200. [[CrossRef](#)]
44. Zhang, S.; Li, F.; Li, T.; Yang, J.; Bu, K.; Chang, L.; Wang, W.; Yan, Y. Remote sensing monitoring of gullies on a regional scale: A case study of Kebai region in Heilongjiang Province, China. *Chin. Geogr. Sci.* **2015**, *25*, 602–611. [[CrossRef](#)]
45. Skytland, N. *Big Data: What is Nasa Doing with Big Data Today*; Open Access Government: Crewe, UK, 2012.
46. Consortium, O.O. *The OpenGIS Abstract Specification-Topic 7: The Earth Imagery Case*; Open Geospatial Consortium, Inc.: Arlington, VA, USA, 1999.
47. Vrieling, A.; Sterk, G.; Vigiak, O. Spatial evaluation of soil erosion risk in the West Usambara Mountains, Tanzania. *Land Degrad. Dev.* **2006**, *17*, 301–319. [[CrossRef](#)]
48. Shruthi, R.B.; Kerle, N.; Jetten, V. Object-based gully feature extraction using high spatial resolution imagery. *Geomorphology* **2011**, *134*, 260–268. [[CrossRef](#)]
49. Chlingaryan, A.; Sukkarieh, S.; Whelan, B. Machine learning approaches for crop yield prediction and nitrogen status estimation in precision agriculture: A review. *Comput. Electron. Agric.* **2018**, *151*, 61–69. [[CrossRef](#)]
50. Zhang, D. *Advances in Machine Learning Applications in Software Engineering*; Igi Global: Hershey, PA, USA, 2006.
51. Karakus, M. Function identification for the intrinsic strength and elastic properties of granitic rocks via genetic programming (GP). *Comput. Geosci.* **2011**, *37*, 1318–1323. [[CrossRef](#)]
52. Ozbek, A.; Unsal, M.; Dikec, A. Estimating uniaxial compressive strength of rocks using genetic expression programming. *J. Rock Mech. Geotech. Eng.* **2013**, *5*, 325–329. [[CrossRef](#)]
53. Vaca, R.A.; Golicher, D.J.; Cayuela, L. Using climatically based random forests to downscale coarse-grained potential natural vegetation maps in tropical Mexico. *Appl. Veg. Sci.* **2011**, *14*, 388–401. [[CrossRef](#)]
54. Périé, C.; de Blois, S. Dominant forest tree species are potentially vulnerable to climate change over large portions of their range even at high latitudes. *PeerJ* **2016**, *4*, e2218. [[CrossRef](#)] [[PubMed](#)]
55. Pouteau, R.; Meyer, J.-Y.; Taputuarai, R.; Stoll, B. Support vector machines to map rare and endangered native plants in Pacific islands forests. *Ecol. Inform.* **2012**, *9*, 37–46. [[CrossRef](#)]
56. Parisouj, P.; Mohebzadeh, H.; Lee, T. Employing Machine Learning Algorithms for Streamflow Prediction: A Case Study of Four River Basins with Different Climatic Zones in the United States. *Water Resour. Manag.* **2020**, *34*, 4113–4131. [[CrossRef](#)]
57. Noymanee, J.; Theeramunkong, T. Flood Forecasting with Machine Learning Technique on Hydrological Modeling. *Procedia Comput. Sci.* **2019**, *156*, 377–386. [[CrossRef](#)]
58. Chen, C.; He, W.; Zhou, H.; Xue, Y.; Zhu, M. A comparative study among machine learning and numerical models for simulating groundwater dynamics in the Heihe River Basin, northwestern China. *Sci. Rep.* **2020**, *10*, 3904. [[CrossRef](#)] [[PubMed](#)]
59. Senthilnath, J.; Dokania, A.; Kandukuri, M.; Ramesh, K.; Anand, G.; Omkar, S. Detection of tomatoes using spectral-spatial methods in remotely sensed RGB images captured by UAV. *Biosyst. Eng.* **2016**, *146*, 16–32. [[CrossRef](#)]
60. Su, Y.-X.; Xu, H.; Yan, L.-J. Support vector machine-based open crop model (SBOCM): Case of rice production in China. *Saudi J. Biol. Sci.* **2017**, *24*, 537–547. [[CrossRef](#)]
61. Kung, H.-Y.; Kuo, T.-H.; Chen, C.-H.; Tsai, P.-Y. Accuracy analysis mechanism for agriculture data using the ensemble neural network method. *Sustainability* **2016**, *8*, 735. [[CrossRef](#)]
62. Arabameri, A.; Chen, W.; Loche, M.; Zhao, X.; Li, Y.; Lombardo, L.; Cerda, A.; Pradhan, B.; Bui, D.T. Comparison of machine learning models for gully erosion susceptibility mapping. *Geosci. Front.* **2019**, *11*, 1609–1620. [[CrossRef](#)]
63. Bui, D.T.; Tuan, T.A.; Klempe, H.; Pradhan, B.; Revhaug, I. Spatial prediction models for shallow landslide hazards: A comparative assessment of the efficacy of support vector machines, artificial neural networks, kernel logistic regression, and logistic model tree. *Landslides* **2016**, *13*, 361–378.
64. Phinzi, K.; Abriha, D.; Bertalan, L.; Holb, I.; Szabó, S. Machine Learning for Gully Feature Extraction Based on a Pan-Sharpended Multispectral Image: Multiclass vs. Binary Approach. *ISPRS Int. J. Geo-Inf.* **2020**, *9*, 252. [[CrossRef](#)]
65. Märker, M.; Pelacani, S.; Schröder, B. A functional entity approach to predict soil erosion processes in a small Plio-Pleistocene Mediterranean catchment in Northern Chianti, Italy. *Geomorphology* **2011**, *125*, 530–540. [[CrossRef](#)]

66. Voyant, C.; Notton, G.; Kalogirou, S.; Nivet, M.-L.; Paoli, C.; Motte, F.; Fouilloy, A. Machine learning methods for solar radiation forecasting: A review. *Renew. Energy* **2017**, *105*, 569–582. [[CrossRef](#)]
67. Liakos, K.G.; Busato, P.; Moshou, D.; Pearson, S.; Bochtis, D. Machine learning in agriculture: A review. *Sensors* **2018**, *18*, 2674. [[CrossRef](#)]
68. Breiman, L. Random forests. *Mach. Learn.* **2001**, *45*, 5–32. [[CrossRef](#)]
69. Amiri, M.; Pourghasemi, H.R.; Ghanbarian, G.A.; Afzali, S.F. Assessment of the importance of gully erosion effective factors using Boruta algorithm and its spatial modeling and mapping using three machine learning algorithms. *Geoderma* **2019**, *340*, 55–69. [[CrossRef](#)]
70. Micheletti, N.; Foresti, L.; Robert, S.; Leuenberger, M.; Pedrazzini, A.; Jaboyedoff, M.; Kanevski, M. Machine learning feature selection methods for landslide susceptibility mapping. *Math. Geosci.* **2014**, *46*, 33–57. [[CrossRef](#)]
71. Liaw, A.; Wiener, M. Classification and regression by randomForest. *R News* **2002**, *2*, 18–22.
72. Pourghasemi, H.R.; Sadhasivam, N.; Kariminejad, N.; Collins, A.L. Gully erosion spatial modelling: Role of machine learning algorithms in selection of the best controlling factors and modelling process. *Geosci. Front.* **2020**, *11*, 2207–2219. [[CrossRef](#)]
73. Naghibi, S.A.; Pourghasemi, H.R.; Dixon, B. GIS-based groundwater potential mapping using boosted regression tree, classification and regression tree, and random forest machine learning models in Iran. *Environ. Monit. Assess.* **2016**, *188*, 44. [[CrossRef](#)] [[PubMed](#)]
74. Wiesmeier, M.; Barthold, F.; Blank, B.; Kögel-Knabner, I. Digital mapping of soil organic matter stocks using Random Forest modeling in a semi-arid steppe ecosystem. *Plant Soil* **2011**, *340*, 7–24. [[CrossRef](#)]
75. Cortes, C.; Vapnik, V. Support-vector networks. *Mach. Learn.* **1995**, *20*, 273–297. [[CrossRef](#)]
76. Mountrakis, G.; Im, J.; Ogole, C. Support vector machines in remote sensing: A review. *ISPRS J. Photogramm. Remote Sens.* **2011**, *66*, 247–259. [[CrossRef](#)]
77. Kavzoglu, T.; Sahin, E.K.; Colkesen, I. Landslide susceptibility mapping using GIS-based multi-criteria decision analysis, support vector machines, and logistic regression. *Landslides* **2014**, *11*, 425–439. [[CrossRef](#)]
78. Kalantar, B.; Pradhan, B.; Naghibi, S.A.; Motevalli, A.; Mansor, S. Assessment of the effects of training data selection on the landslide susceptibility mapping: A comparison between support vector machine (SVM), logistic regression (LR) and artificial neural networks (ANN). *Geomat. Nat. Hazards Risk* **2018**, *9*, 49–69. [[CrossRef](#)]
79. Basak, D.; Pal, S.; Patranabis, D.C. Support vector regression. *Neural Inf. Process.-Lett. Rev.* **2007**, *11*, 203–224.
80. Vapnik, V. *The Nature of Statistical Learning Theory*; Springer Science & Business Media: Berlin/Heidelberg, Germany, 2013.
81. Bui, D.T.; Pradhan, B.; Lofman, O.; Revhaug, I.; Dick, O.B. Landslide susceptibility assessment in the Hoa Binh province of Vietnam: A comparison of the Levenberg–Marquardt and Bayesian regularized neural networks. *Geomorphology* **2012**, *171*, 12–29.
82. Pradhan, B. A comparative study on the predictive ability of the decision tree, support vector machine and neuro-fuzzy models in landslide susceptibility mapping using GIS. *Comput. Geosci.* **2013**, *51*, 350–365. [[CrossRef](#)]
83. Freund, Y.; Mason, L. The alternating decision tree learning algorithm. In Proceedings of the ICML, Bled, Slovenia, 27–30 June 1999; pp. 124–133.
84. Sok, H.K.; Ooi, M.P.-L.; Kuang, Y.C.; Demidenko, S. Multivariate alternating decision trees. *Pattern Recognit.* **2016**, *50*, 195–209. [[CrossRef](#)]
85. Pham, B.T.; Bui, D.T.; Prakash, I. Landslide susceptibility assessment using bagging ensemble based alternating decision trees, logistic regression and J48 decision trees methods: A comparative study. *Geotech. Geol. Eng.* **2017**, *35*, 2597–2611. [[CrossRef](#)]
86. Farid, D.M.; Zhang, L.; Rahman, C.M.; Hossain, M.A.; Strachan, R. Hybrid decision tree and naïve Bayes classifiers for multi-class classification tasks. *Expert Syst. Appl.* **2014**, *41*, 1937–1946. [[CrossRef](#)]
87. Wang, L.-M.; Li, X.-L.; Cao, C.-H.; Yuan, S.-M. Combining decision tree and Naive Bayes for classification. *Knowl.-Based Syst.* **2006**, *19*, 511–515. [[CrossRef](#)]
88. Kohavi, R. Scaling up the accuracy of naive-bayes classifiers: A decision-tree hybrid. In Proceedings of the Kdd, Portland, OR, USA, 2–4 August 1996; pp. 202–207.
89. Chen, W.; Shirzadi, A.; Shahabi, H.; Ahmad, B.B.; Zhang, S.; Hong, H.; Zhang, N. A novel hybrid artificial intelligence approach based on the rotation forest ensemble and naïve Bayes tree classifiers for a landslide susceptibility assessment in Langao County, China. *Geomat. Nat. Hazards Risk* **2017**, *8*, 1955–1977. [[CrossRef](#)]
90. Landwehr, N.; Hall, M.; Frank, E. Logistic model trees. *Mach. Learn.* **2005**, *59*, 161–205. [[CrossRef](#)]
91. Heung, B.; Hodúl, M.; Schmidt, M.G. Comparing the use of training data derived from legacy soil pits and soil survey polygons for mapping soil classes. *Geoderma* **2017**, *290*, 51–68. [[CrossRef](#)]
92. Chen, W.; Xie, X.; Wang, J.; Pradhan, B.; Hong, H.; Bui, D.T.; Duan, Z.; Ma, J. A comparative study of logistic model tree, random forest, and classification and regression tree models for spatial prediction of landslide susceptibility. *Catena* **2017**, *151*, 147–160. [[CrossRef](#)]
93. Chen, W.; Pradhan, B.; Li, S.; Shahabi, H.; Rizeei, H.M.; Hou, E.; Wang, S. Novel hybrid integration approach of bagging-based fisher’s linear discriminant function for groundwater potential analysis. *Nat. Resour. Res.* **2019**, *28*, 1239–1258. [[CrossRef](#)]
94. Breiman, L.; Friedman, J.; Olshen, R.; Stone, C. Classification and regression trees. *Biometrics* **1984**, *40*, 358–361.
95. Lee, S.; Jun, C.-H. Fast incremental learning of logistic model tree using least angle regression. *Expert Syst. Appl.* **2018**, *97*, 137–145. [[CrossRef](#)]

96. Wang, L.-J.; Guo, M.; Sawada, K.; Lin, J.; Zhang, J. A comparative study of landslide susceptibility maps using logistic regression, frequency ratio, decision tree, weights of evidence and artificial neural network. *Geosci. J.* **2016**, *20*, 117–136. [[CrossRef](#)]
97. Kadavi, P.R.; Lee, C.-W.; Lee, S. Landslide-susceptibility mapping in Gangwon-do, South Korea, using logistic regression and decision tree models. *Environ. Earth Sci.* **2019**, *78*, 116. [[CrossRef](#)]
98. Rahmati, O.; Tahmasebipour, N.; Haghizadeh, A.; Pourghasemi, H.R.; Feizizadeh, B. Evaluation of different machine learning models for predicting and mapping the susceptibility of gully erosion. *Geomorphology* **2017**, *298*, 118–137. [[CrossRef](#)]
99. Ermini, L.; Catani, F.; Casagli, N. Artificial neural networks applied to landslide susceptibility assessment. *Geomorphology* **2005**, *66*, 327–343. [[CrossRef](#)]
100. Zare, M.; Pourghasemi, H.R.; Vafakhah, M.; Pradhan, B. Landslide susceptibility mapping at Vaz Watershed (Iran) using an artificial neural network model: A comparison between multilayer perceptron (MLP) and radial basic function (RBF) algorithms. *Arab. J. Geosci.* **2013**, *6*, 2873–2888. [[CrossRef](#)]
101. Gorsevski, P.V.; Brown, M.K.; Panter, K.; Onasch, C.M.; Simic, A.; Snyder, J. Landslide detection and susceptibility mapping using LiDAR and an artificial neural network approach: A case study in the Cuyahoga Valley National Park, Ohio. *Landslides* **2016**, *13*, 467–484. [[CrossRef](#)]
102. Yegnanarayana, B. *Artificial Neural Networks*; PHI Learning Pvt. Ltd.: Delhi, India, 2009.
103. Peethambaran, B.; Anbalagan, R.; Kanungo, D.; Goswami, A.; Shihabudheen, K. A comparative evaluation of supervised machine learning algorithms for township level landslide susceptibility zonation in parts of Indian Himalayas. *CATENA* **2020**, *195*, 104751. [[CrossRef](#)]
104. Bishop, C.M. *Neural Networks for Pattern Recognition*; Oxford University Press: Oxford, UK, 1995.
105. Shen, C.; Wang, L.; Li, Q. Optimization of injection molding process parameters using combination of artificial neural network and genetic algorithm method. *J. Mater. Process. Technol.* **2007**, *183*, 412–418. [[CrossRef](#)]
106. Choi, J.; Oh, H.-J.; Lee, H.-J.; Lee, C.; Lee, S. Combining landslide susceptibility maps obtained from frequency ratio, logistic regression, and artificial neural network models using ASTER images and GIS. *Eng. Geol.* **2012**, *124*, 12–23. [[CrossRef](#)]
107. Lyashevskaya, O.; Harma, C.; Minto, C.; Clarke, M.; Brophy, D. Long-term trends in herring growth primarily linked to temperature by gradient boosting regression trees. *Ecol. Inform.* **2020**, *60*, 101154. [[CrossRef](#)]
108. Aertsen, W.; Kint, V.; Van Orshoven, J.; Özkan, K.; Muys, B. Comparison and ranking of different modelling techniques for prediction of site index in Mediterranean mountain forests. *Ecol. Model.* **2010**, *221*, 1119–1130. [[CrossRef](#)]
109. Hu, Y.; Dai, Z.; Guldman, J.-M. Modeling the impact of 2D/3D urban indicators on the urban heat island over different seasons: A boosted regression tree approach. *J. Environ. Manag.* **2020**, *266*, 110424. [[CrossRef](#)] [[PubMed](#)]
110. Sayegh, A.; Tate, J.E.; Ropkins, K. Understanding how roadside concentrations of NO_x are influenced by the background levels, traffic density, and meteorological conditions using Boosted Regression Trees. *Atmos. Environ.* **2016**, *127*, 163–175. [[CrossRef](#)]
111. Zhang, W.; Du, Z.; Zhang, D.; Yu, S.; Hao, Y. Boosted regression tree model-based assessment of the impacts of meteorological drivers of hand, foot and mouth disease in Guangdong, China. *Sci. Total Environ.* **2016**, *553*, 366–371. [[CrossRef](#)] [[PubMed](#)]
112. Froeschke, J.T.; Froeschke, B.F. Spatio-temporal predictive model based on environmental factors for juvenile spotted seatrout in Texas estuaries using boosted regression trees. *Fish. Res.* **2011**, *111*, 131–138. [[CrossRef](#)]
113. Shruthi, R.B.; Kerle, N.; Jetten, V.; Stein, A. Object-based gully system prediction from medium resolution imagery using Random Forests. *Geomorphology* **2014**, *216*, 283–294. [[CrossRef](#)]
114. Angileri, S.E.; Conoscenti, C.; Hochschild, V.; Märker, M.; Rotigliano, E.; Agnesi, V. Water erosion susceptibility mapping by applying stochastic gradient treeboost to the Imera Meridionale river basin (Sicily, Italy). *Geomorphology* **2016**, *262*, 61–76. [[CrossRef](#)]
115. Garosi, Y.; Sheklabadi, M.; Conoscenti, C.; Pourghasemi, H.R.; Van Oost, K. Assessing the performance of GIS-based machine learning models with different accuracy measures for determining susceptibility to gully erosion. *Sci. Total Environ.* **2019**, *664*, 1117–1132. [[CrossRef](#)] [[PubMed](#)]
116. Makaya, N.P.; Mutanga, O.; Kiala, Z.; Dube, T.; Seutloali, K.E. Assessing the potential of Sentinel-2 MSI sensor in detecting and mapping the spatial distribution of gullies in a communal grazing landscape. *Phys. Chem. Earth Parts A/B/C* **2019**, *112*, 66–74. [[CrossRef](#)]
117. Gayen, A.; Pourghasemi, H.R.; Saha, S.; Keesstra, S.; Bai, S. Gully erosion susceptibility assessment and management of hazard-prone areas in India using different machine learning algorithms. *Sci. Total Environ.* **2019**, *668*, 124–138. [[CrossRef](#)] [[PubMed](#)]
118. Arabameri, A.; Pradhan, B.; Rezaei, K. Gully erosion zonation mapping using integrated geographically weighted regression with certainty factor and random forest models in GIS. *J. Environ. Manag.* **2019**, *232*, 928–942. [[CrossRef](#)]
119. Arabameri, A.; Cerda, A.; Pradhan, B.; Tiefenbacher, J.P.; Lombardo, L.; Bui, D.T. A methodological comparison of head-cut based gully erosion susceptibility models: Combined use of statistical and artificial intelligence. *Geomorphology* **2020**, *359*, 107136. [[CrossRef](#)]
120. Arabameri, A.; Sadhasivam, N.; Turabieh, H.; Mafarja, M.; Rezaie, F.; Pal, S.C.; Santosh, M. Credal decision tree based novel ensemble models for spatial assessment of gully erosion and sustainable management. *Sci. Rep.* **2021**, *11*, 3147. [[CrossRef](#)] [[PubMed](#)]
121. Roy, J.; Saha, S. Integration of artificial intelligence with meta classifiers for the gully erosion susceptibility assessment in Hinglo river basin, Eastern India. *Adv. Space Res.* **2021**, *67*, 316–333. [[CrossRef](#)]

122. Chowdhuri, I.; Pal, S.C.; Saha, A.; Chakraborty, R.; Roy, P. Evaluation of different DEMs for gully erosion susceptibility mapping using in-situ field measurement and validation. *Ecol. Inform.* **2021**, *65*, 101425. [[CrossRef](#)]
123. Wang, F.; Sahana, M.; Pahlevanzadeh, B.; Pal, S.C.; Shit, P.K.; Piran, M.J.; Janizadeh, S.; Band, S.S.; Mosavi, A. Applying different resampling strategies in machine learning models to predict head-cut gully erosion susceptibility. *Alex. Eng. J.* **2021**, *60*, 5813–5829. [[CrossRef](#)]
124. Arabameri, A.; Rezaie, F.; Pal, S.C.; Cerda, A.; Saha, A.; Chakraborty, R.; Lee, S. Modelling of piping collapses and gully headcut landforms: Evaluating topographic variables from different types of DEM. *Geosci. Front.* **2021**, *12*, 101230. [[CrossRef](#)]
125. Yang, A.; Wang, C.; Pang, G.; Long, Y.; Wang, L.; Cruse, R.M.; Yang, Q. Gully Erosion Susceptibility Mapping in Highly Complex Terrain Using Machine Learning Models. *ISPRS Int. J. Geo-Inf.* **2021**, *10*, 680. [[CrossRef](#)]
126. Süzen, M.L.; Doyuran, V. A comparison of the GIS based landslide susceptibility assessment methods: Multivariate versus bivariate. *Environ. Geol.* **2004**, *45*, 665–679. [[CrossRef](#)]
127. Schicker, R.; Moon, V. Comparison of bivariate and multivariate statistical approaches in landslide susceptibility mapping at a regional scale. *Geomorphology* **2012**, *161*, 40–57. [[CrossRef](#)]
128. Dou, J.; Yamagishi, H.; Pourghasemi, H.R.; Yunus, A.P.; Song, X.; Xu, Y.; Zhu, Z. An integrated artificial neural network model for the landslide susceptibility assessment of Osado Island, Japan. *Nat. Hazards* **2015**, *78*, 1749–1776. [[CrossRef](#)]
129. Rahmati, O.; Haghizadeh, A.; Pourghasemi, H.R.; Noormohamadi, F. Gully erosion susceptibility mapping: The role of GIS-based bivariate statistical models and their comparison. *Nat. Hazards* **2016**, *82*, 1231–1258. [[CrossRef](#)]
130. Conoscenti, C.; Di Maggio, C.; Rotigliano, E. Soil erosion susceptibility assessment and validation using a geostatistical multivariate approach: A test in Southern Sicily. *Nat. Hazards* **2008**, *46*, 287–305. [[CrossRef](#)]
131. Jahantigh, M.; Pessarakli, M. Causes and effects of gully erosion on agricultural lands and the environment. *Commun. Soil Sci. Plant Anal.* **2011**, *42*, 2250–2255. [[CrossRef](#)]
132. Kheir, R.B.; Wilson, J.; Deng, Y. Use of terrain variables for mapping gully erosion susceptibility in Lebanon. *Earth Surf. Process. Landf. J. Br. Geomorphol. Res. Group* **2007**, *32*, 1770–1782. [[CrossRef](#)]
133. Wells, R.R.; Bennett, S.J.; Alonso, C.V. Effect of soil texture, tailwater height, and pore-water pressure on the morphodynamics of migrating headcuts in upland concentrated flows. *Earth Surf. Process. Landf. J. Br. Geomorphol. Res. Group* **2009**, *34*, 1867–1877. [[CrossRef](#)]
134. Agnesi, V.; Angileri, S.; Cappadonia, C.; Conoscenti, C.; Rotigliano, E. Multi parametric gis analysis to assess gully erosion susceptibility: A test in southern sicily, italy. *Landf. Anal.* **2011**, *17*, 15–20.
135. Conoscenti, C.; Agnesi, V.; Angileri, S.; Cappadonia, C.; Rotigliano, E.; Märker, M. A GIS-based approach for gully erosion susceptibility modelling: A test in Sicily, Italy. *Environ. Earth Sci.* **2013**, *70*, 1179–1195. [[CrossRef](#)]
136. Mararakanye, N.; Sumner, P.D. Gully erosion: A comparison of contributing factors in two catchments in South Africa. *Geomorphology* **2017**, *288*, 99–110. [[CrossRef](#)]
137. Pourghasemi, H.R.; Yousefi, S.; Kornejady, A.; Cerdà, A. Performance assessment of individual and ensemble data-mining techniques for gully erosion modeling. *Sci. Total Environ.* **2017**, *609*, 764–775. [[CrossRef](#)] [[PubMed](#)]
138. Rahmati, O.; Tahmasebipour, N.; Haghizadeh, A.; Pourghasemi, H.R.; Feizizadeh, B. Evaluating the influence of geo-environmental factors on gully erosion in a semi-arid region of Iran: An integrated framework. *Sci. Total Environ.* **2017**, *579*, 913–927. [[CrossRef](#)] [[PubMed](#)]
139. Gutiérrez, Á.G.; Schnabel, S.; Contador, F.L. Gully erosion, land use and topographical thresholds during the last 60 years in a small rangeland catchment in SW Spain. *Land Degrad. Dev.* **2009**, *20*, 535–550. [[CrossRef](#)]
140. Shahin, K.A.; Hassan, N. Sources of shared variability among body shape characters at marketing age in New Zealand White and Egyptian rabbit breeds. In *Annales de Zootechnie*; EDP Sciences: Les Ulis, France, 2000; pp. 435–445.
141. Bui, D.T.; Pradhan, B.; Lofman, O.; Revhaug, I.; Dick, O.B. Spatial prediction of landslide hazards in Hoa Binh province (Vietnam): A comparative assessment of the efficacy of evidential belief functions and fuzzy logic models. *Catena* **2012**, *96*, 28–40.
142. Guzzetti, F.; Reichenbach, P.; Ardizzone, F.; Cardinali, M.; Galli, M. Estimating the quality of landslide susceptibility models. *Geomorphology* **2006**, *81*, 166–184. [[CrossRef](#)]
143. Landis, J.R.; Koch, G.G. The measurement of observer agreement for categorical data. *Biometrics* **1977**, *33*, 159–174. [[CrossRef](#)]
144. Bradley, A.P. The use of the area under the ROC curve in the evaluation of machine learning algorithms. *Pattern Recognit.* **1997**, *30*, 1145–1159. [[CrossRef](#)]
145. Egan, J.P.; Egan, J.P. *Signal Detection Theory and ROC-Analysis*; Academic press: Cambridge, MA, USA, 1975.
146. Mandrekar, J.N. Receiver operating characteristic curve in diagnostic test assessment. *J. Thorac. Oncol.* **2010**, *5*, 1315–1316. [[CrossRef](#)] [[PubMed](#)]
147. Hajian-Tilaki, K. Receiver operating characteristic (ROC) curve analysis for medical diagnostic test evaluation. *Casp. J. Intern. Med.* **2013**, *4*, 627.
148. Yesilnacar, E.; Topal, T. Landslide susceptibility mapping: A comparison of logistic regression and neural networks methods in a medium scale study, Hendek region (Turkey). *Eng. Geol.* **2005**, *79*, 251–266. [[CrossRef](#)]
149. Svoray, T.; Michailov, E.; Cohen, A.; Rokah, L.; Sturm, A. Predicting gully initiation: Comparing data mining techniques, analytical hierarchy processes and the topographic threshold. *Earth Surf. Process. Landf.* **2012**, *37*, 607–619. [[CrossRef](#)]

150. Fernandes, J.; Bateira, C.; Soares, L.; Faria, A.; Oliveira, A.; Hermenegildo, C.; Moura, R.; Gonçalves, J. SIMWE model application on susceptibility analysis to bank gully erosion in Alto Douro Wine Region agricultural terraces. *Catena* **2017**, *153*, 39–49. [[CrossRef](#)]
151. Kuhnert, P.M.; Henderson, A.K.; Bartley, R.; Herr, A. Incorporating uncertainty in gully erosion calculations using the random forests modelling approach. *Environmetrics* **2010**, *21*, 493–509. [[CrossRef](#)]
152. Zhang, X.; Fan, J.; Liu, Q.; Xiong, D. The contribution of gully erosion to total sediment production in a small watershed in Southwest China. *Phys. Geogr.* **2018**, *39*, 246–263. [[CrossRef](#)]
153. Arabameri, A.; Rezaei, K.; Pourghasemi, H.R.; Lee, S.; Yamani, M. GIS-based gully erosion susceptibility mapping: A comparison among three data-driven models and AHP knowledge-based technique. *Environ. Earth Sci.* **2018**, *77*, 628. [[CrossRef](#)]
154. Kantardzic, M. *Data Mining: Concepts, Models, Methods, and Algorithms*; John Wiley & Sons: New York, NY, USA, 2011.
155. Marjanović, M.; Kovačević, M.; Bajat, B.; Voženilek, V. Landslide susceptibility assessment using SVM machine learning algorithm. *Eng. Geol.* **2011**, *123*, 225–234. [[CrossRef](#)]
156. Xu, C.; Dai, F.; Xu, X.; Lee, Y.H. GIS-based support vector machine modeling of earthquake-triggered landslide susceptibility in the Jianjiang River watershed, China. *Geomorphology* **2012**, *145*, 70–80. [[CrossRef](#)]
157. Goh, A.T.; Goh, S. Support vector machines: Their use in geotechnical engineering as illustrated using seismic liquefaction data. *Comput. Geotech.* **2007**, *34*, 410–421. [[CrossRef](#)]
158. Samui, P. Support vector classifier analysis of slope. *Geomat. Nat. Hazards Risk* **2013**, *4*, 1–12. [[CrossRef](#)]